PROCEEDINGS OF SPIE

SPIEDigitalLibrary.org/conference-proceedings-of-spie

Radiative cooling for concentrating photovoltaic systems

Yubo Sun, Zhiguang Zhou, Xin Jin, Xingshu Sun, Muhammad Ashraful Alam, et al.

Yubo Sun, Zhiguang Zhou, Xin Jin, Xingshu Sun, Muhammad Ashraful Alam, Peter Bermel, "Radiative cooling for concentrating photovoltaic systems," Proc. SPIE 10369, Thermal Radiation Management for Energy Applications, 103690D (6 September 2017); doi: 10.1117/12.2273916

SPIE.

Event: SPIE Optical Engineering + Applications, 2017, San Diego, California, United States

Radiative cooling for concentrating photovoltaic systems

Yubo Sun[1,*], Zhiguang Zhou[1,2*], Xin Jin[1], Xingshu Sun[1], Muhammad Ashraful Alam[1], Peter Bermel[1,2,†]

[1] School of Electrical & Computer Engineering, Purdue University, West Lafayette, IN, USA 47907
[2] Birck Nanotechnology Center, Purdue University, West Lafayette, IN, USA 47907

ABSTRACT

Radiative cooling, a unique and uncommon passive cooling method for devices operating outdoors, has recently been demonstrated to be effective for photovoltaic thermal management. In this work, we investigate the effect of radiative cooling as a complement to existing passive cooling methods like convective cooling in a related system with much higher heat loads: a high-concentration photovoltaic (HCPV) system. A feasible radiative cooler design addressing the thermal management challenges here is proposed. It consists of low-iron soda-lime glass with a porous layer on top as an anti-reflection coating and a diamond layer as heat spreader. It is found that the proposed structure has strong mid-IR emittance as well as high solar transmission, allowing radiative cooling under direct sunlight and low loss in the concentrated solar irradiance. A systematic simulation with realistic considerations is then performed. Compared with a conventional copper cooler, the lowest temperature reached by the proposed radiative cooler is $14\ \mathrm{K}$ lower. Furthermore, less area of the proposed cooler is needed to reach a standard target temperature ($333.15\ \mathrm{K}$) for steady-state operation under high concentrations for the crystalline silicon PV module. In order to compare the coolers quantitatively, a figure of merit – cooling power per weight - is introduced. At the target temperature, the proposed cooler is determined to have a cooling power per weight of $75\ \mathrm{W/kg}$, around 3.7 times higher than that of the conventional copper cooler.

Keywords: radiative cooling, concentrating photovoltaics, thermal radiation, convective cooling

INTRODUCTION

Radiative cooling is a passive cooling mechanism that dissipates heat via thermal radiation. For outdoor applications, the cold universe at $3\ \mathrm{K}$ can be accessed through the sky as the heat sink if the cooler has thermal emission within the wavelength range of $8-13\ \mu\mathrm{m}$ [1–3]. In this range, known as the atmospheric window, the atmosphere has high transmission allowing transmission of the radiation from the ground. The existence of the atmospheric window makes outdoor radiative cooling a unique passive cooling method that in principle can reach below-ambient temperature. The challenge is therefore to find cooler materials that have strong thermal emittance within $8-13\ \mu\mathrm{m}$, and much lower thermal emittance outside this window. Fortunately, early works showed that natural bulk materials such as polyvinyl fluoride [2,4], silicon monoxide (SiO) [3] and silicon nitride (Si_3N_4) [5] are suitable for radiative cooling. Composite materials such as SiO_2 and SiC nanoparticles in polyethylene binder [6] were later proposed as alternative cooler materials. Recent progress in nanophotonics allows the emittance spectra of bulk materials to be tailored by photonic crystal structures [7,8]. It has recently been demonstrated experimentally that nanophotonic coolers can reach below ambient temperatures, even under direct sunlight [9]. When placed in vacuum, such nanophotonic coolers have been shown to reach sub-freezing cooling [10]. More recently, a high-performance metamaterial based radiative cooler has been demonstrated; the researchers conducting the experiment believe that it may be a candidate for mass production [11].

Radiative cooling can potentially be applied to address the increasing demands of electronic device cooling. For instance, it has recently been demonstrated that a 2D photonic crystal silica cooler can effectively cool down the bare solar cell underneath [12]. For an optoelectronic device with higher heat loads, known as thermophotovoltaics, radiative cooling with low-iron soda lime 2D photonic crystal cooler was shown to be effective [13]. There are many other outdoor electronics that could benefit from radiative cooling. Thus, it is important to explore the possibility of using radiative cooling as either a major or a complementary cooling method for these applications.

---

[*] Both of these authors contributed equally to this work.
[†] Corresponding author. Email address: pbermel@purdue.edu

Thermal Radiation Management for Energy Applications, edited by Peter Bermel, Mowafak M. Al-Jassim, Proc. of SPIE Vol. 10369, 103690D · © 2017 SPIE
CCC code: 0277-786X/17/$18 · doi: 10.1117/12.2273916

In this work, we investigate the application of radiative cooling on high-concentration photovoltaic (HCPV) systems. Due to the highly concentrated solar irradiance and strongly temperature dependent photovoltaic (PV) performance, cooling is one of the major challenges in HCPV research [14]. Operating at high temperatures not only reduces the initial solar-to-electricity conversion efficiency, but can also significantly reduce the long-term reliability, which plays a major role in determining the levelized cost of energy for these systems [15]. Most works focus on engineering the heat sink design to enhance convection cooling [16–18]. Although radiative heat transfer has been brought to increased attention recently [14], radiative cooling through the atmospheric window has not been investigated much in the context of HCPV. In this work, we consider HCPV systems with parabolic reflectors concentrating the sunlight, with the PV module facing toward the ground. We show that a transparent dielectric radiative cooler, referred to as the multi-layer low-iron soda lime glass cooler, on the backside of the PV module can have effective cooling without using more area than the PV module and the concentrator optics. The performance of the HCPV system with radiative cooling is evaluated by a realistic calculation framework. Details of the framework will be introduced in Section 2. In Section 3, the radiative cooler design will be discussed, followed by the calculation results. The proposed cooler will then be compared with a conventional flat copper cooler. To compare the two coolers quantitatively, we introduce a figure of merit, cooling power per weight, which captures both the capability of heat dissipation and the weight of the cooler.

CALCULATION FRAMEWORK

To fully assess the radiative cooling effect on HCPV systems, we establish an optical-thermal-electrical coupled simulation framework based on power balance to self-consistently find the equilibrium temperature of the HCPV system. As depicted in Fig. 1(A), the entire HCPV setup consists of three major parts: a radiative cooler on top facing towards the sky, a parabolic reflector at the bottom near the ground that reflects and concentrates sunlight, and a silicon-based PV module underneath the radiative cooler that absorbs concentrated sunlight. Compared to III-V multi-junction PV modules, silicon-based PV modules may not be as efficient at high concentrations (> 100 suns) because of Auger recombination [19]; thus, using models developed for the former may undervalue the value of radiative cooling. In future work, the PV model will be adjusted to predict electric output power and the resulting radiative cooling more precisely at high concentrations. Nonetheless, if we consider the radiative cooler and PV module as a whole, a power balance equation governs the heat transfer inflow and outflow of the system in steady state, which is as follows:

$$P_{in}^{PV} + P_{in}^{cool} = P_{out}^{PV} + P_{out}^{cool} + P_{non-rad}^{PV,cool}, \tag{1}$$

where P_{in}^{PV} is the total absorbed radiative power by the PV module; P_{in}^{cool} is the total absorbed radiative power by the radiative cooler; P_{out}^{PV} is the radiative and electrical output power from the PV module; P_{out}^{cool} is the total power radiated out from the cooler and $P_{non-rad}^{PV,cool}$ denotes non-radiative heat transfer. The power balance equation, Eq. (1), is similar to the one used in [13], but is modified to include double-side radiation from the cooler and a realistic silicon-based PV module.

The total absorbed radiative power by the PV module has three contributions: (1) the solar power absorbed by the PV module P_{sun}^{PV}, (2) the multiple bounces of thermal radiation from PV module and back onto PV module again P_{rad-PV}^{PV}, and (3) the emission from the parabolic reflector absorbed by the PV module P_{R}^{PV}. Thus, the expression of P_{in}^{PV} is given as follows:

$$P_{in}^{PV} = P_{sun}^{PV} + P_{rad-PV}^{PV} + P_{R}^{PV}, \tag{2}$$

Since the thermal radiation of PV module under the range of temperature considered in this work is low and the view factor from the reflector to the module is close to zero, the latter two terms in Eq. (2) are negligible. While P_{sun}^{PV} can be expressed as:

$$P_{sun}^{PV} = C \cdot \rho_R \cdot A_{PV} \cdot \int d\lambda\, \varepsilon_{PV}(\lambda)\left[\frac{A_{cool} - A_{PV}}{A_R - A_{PV}}\tau_{cool}(\lambda, 0) + \left(1 - \frac{A_{cool} - A_{PV}}{A_R - A_{PV}}\right)\right] I_{AM1.5D}(\lambda), \tag{3}$$

in which C is the nominal concentration factor determined by the area ratio of the concentrator footprint and the module ; $I_{AM1.5D}(\lambda)$ is the AM1.5D spectrum; The actual concentration factor can be derived as $C_{actual} =$

$C \cdot \rho_R \cdot [\frac{A_{cool}-A_{PV}}{A_R-A_{PV}}\tau_{cool}(\lambda,0) + (1-\frac{A_{cool}-A_{PV}}{A_R-A_{PV}})]$; $\rho_R = 0.9$ is the reflectivity of the parabolic reflector; A_{cool} is the surface area of the radiative cooler; $A_{PV} = 1\ \text{cm}^2$ is the PV module area; A_R is the footprint area of the parabolic reflector; $\varepsilon_{PV}(\lambda)$ is the spectral dependent PV module emittance and $\tau_{cool}(\lambda,0)$ represents the transmittance spectrum of the radiative cooler at normal incident angle.

The power output from the PV module P_{out}^{PV} is comprised of two terms P_{ele}^{PV} and P_{rad}^{PV} as Eq. (4):

$$P_{out}^{PV} = P_{ele}^{PV} + P_{rad}^{PV}, \tag{4}$$

$$P_{ele}^{PV} = \eta(C_{actual},T)\cdot C\cdot\rho_R\cdot A_{PV}\cdot\int d\lambda\,[\frac{A_{cool}-A_{PV}}{A_R-A_{PV}}\tau_{cool}(\lambda,0)+(1-\frac{A_{cool}-A_{PV}}{A_R-A_{PV}})]I_{AM1.5D}(\lambda), \tag{5}$$

$$P_{rad}^{PV} = A_{PV}\cdot\int d\Omega\,cos\theta\int d\lambda\,\varepsilon_{PV}(\lambda)I_{BB}(\lambda,T_{PV}) \tag{6}$$

The electrical power output from the module is calculated by Eq. (5), where $\eta(C_{actual},T)$ is temperature and concentration factor dependent PV module efficiency attained by physics-based drift-diffusion solver TCAD Sentaurus calibrated against the record efficiency of HIT solar cells at one sun under room temperature [$\eta(1\ \text{sun}, 300\ \text{K}) = 24.7\%$][20]. The radiative power output term P_{rad}^{PV} is calculated by Eq. (6), where $I_{BB}(\lambda,T) = (2hc^2)/[\lambda^5(\exp(hc/\lambda kT)-1)]$ is the Planck's blackbody radiation function, and T_{PV} is the temperature of the PV module.

For the radiative cooler, the total absorbed power P_{in}^{cool} can be expanded into four terms, as follows:

$$P_{in}^{cool} = P_{atm}^{cool-up} + P_{sun}^{cool} + P_G^{cool} + P_{rad-PV}^{cool}, \tag{7}$$

$$P_{atm}^{cool-up} = A_{cool}\cdot\int d\Omega\,cos\theta\int d\lambda\,\varepsilon_{cool}(\lambda,\theta)\varepsilon_{atm}(\lambda,\theta)I_{BB}(\lambda,T_a), \tag{8}$$

$$P_{sun}^{cool} = A_{cool}\cdot\int d\lambda\,\varepsilon_{cool}(\lambda,0)I_{AM1.5G}(\lambda), \tag{9}$$

$$P_G^{cool} = (A_{cool}-A_{PV})\cdot F_{cool-G}\cdot\varepsilon_G\cdot\int d\Omega\,cos\theta\int d\lambda\,I_{BB}(\lambda,T_a)\varepsilon'_{cool}(\lambda,\theta), \tag{10}$$

where $P_{atm}^{cool-up}$, calculated by Eq. (8), is the atmospheric radiation absorbed by the top surface of the cooler, in which $\varepsilon_{cool}(\lambda,\theta)$ and $\varepsilon_{atm}(\lambda,\theta)$ are spectral and angular dependent emittance of the top surface of radiative cooler and atmosphere, respectively. $\varepsilon_{atm}(\lambda,\theta)$ is calculated by MODTRAN (Mid-latitude winter) atmospheric transmittance data $\tau_{atm}(\lambda,0)$ with angular modulation: $\varepsilon_{atm}(\lambda,\theta) = 1-\tau_{atm}(\lambda,0)^{\,1/\cos\theta\ 3}$; $T_a = 293.15$ K is the ambient temperature[14]. P_{sun}^{cool}, calculated by Eq. (9), is the solar power absorption by the radiative cooler. It should be noted that the solar irradiance used for this term should be the AM1.5G spectrum. P_G^{cool}, calculated by Eq. (10), is the ground emission absorbed by the bottom surface of the radiative cooler, in which F_{cool-G} is the view factor from the radiative cooler to ground and is assumed to be 0.9; ε_G is the ground emissivity, calculated from a diffusive ground albedo presumed to be 0.1, a common value for soil [21]; $\varepsilon'_{cool}(\lambda,\theta)$ is the emittance of the bottom surface of the radiative cooler. The last term in Eq. (7) can be neglected, since the PV module and the cooler are close to thermal equilibrium.

The thermal radiation outflow from the cooler P_{out}^{cool} is composed of two terms, namely the upward and downward thermal radiation P_{rad-up}^{cool} and $P_{rad-down}^{cool}$, given below:

$$P_{out}^{cool} = P_{rad-up}^{cool} + P_{rad-down}^{cool}, \tag{11}$$

$$P_{rad-up}^{cool} = A_{cool} \cdot \int d\Omega \, cos\theta \int d\lambda \, \varepsilon_{cool}(\lambda,\theta) I_{BB}(\lambda, T_{cool}), \tag{12}$$

$$P_{rad-down}^{cool} = (A_{cool} - A_{PV}) \cdot F_{cool-G} \cdot \varepsilon_G \cdot \int d\Omega \, cos\theta \int d\lambda \, \varepsilon'_{cool}(\lambda,\theta) I_{BB}(\lambda, T_{cool}), \tag{13}$$

In both equations above, T_{cool} is the cooler temperature.

The aforementioned non-radiative heat transfer term of the system $P_{non-rad}^{PV,cool}$ is simply the convective heat transfer at the top and bottom surfaces, with uniform temperature assumed between the cooler and PV modules (i.e., $T_{cool} = T_{PV}$):

$$P_{non-rad}^{PV,cool} = 2 \cdot h \cdot A_{cool}(T_{PV} - T_a), \tag{14}$$

where the convection coefficient $h = 5$ W/m^{2}K [14].

The overall scheme of the simulation framework is illustrated in Fig. 1(B). To solve the equilibrium temperature of the PV module, we begin by guessing the initial temperature of the PV module (T_{PV}) and calculating the power flow of each corresponding heat transfer terms to validate the power balanced equation Eq. (1). If not satisfied, a new T_{PV} will be assigned and tested until it self-consistently concurred with power balanced equation. The calculation framework has been benchmarked against the calculation method in [14], which is also consistent with the experiments presented in [22]. Further validation by an experiment closer to the HCPV system modeled here would be warranted.

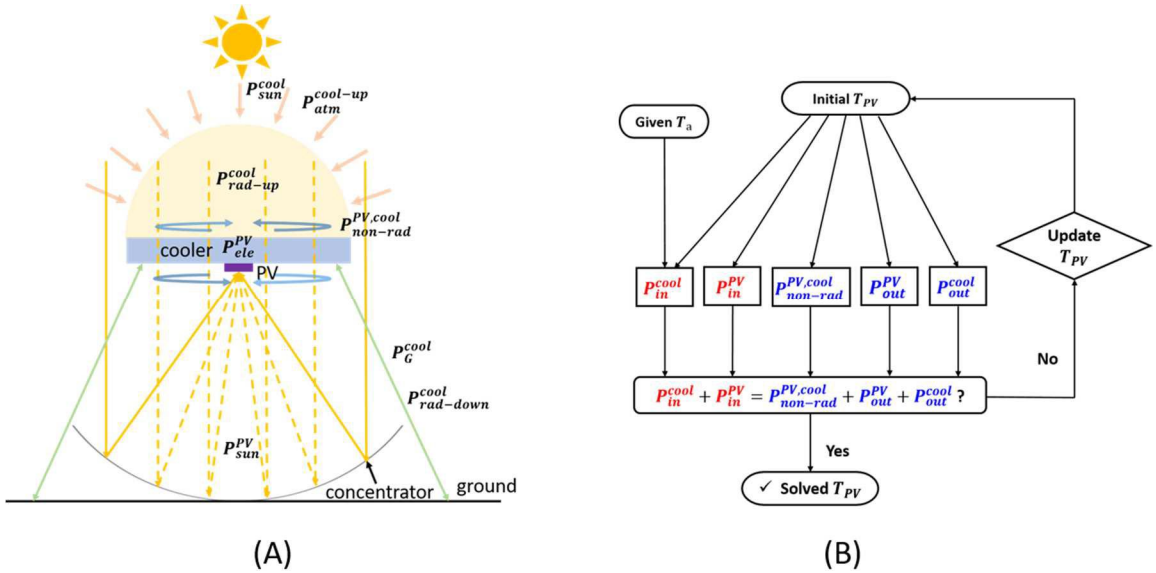

Figure 1. (A). Schematic of a high-concentration photovoltaic (HCPV) system with radiative cooling. The HCPV has a parabolic reflector as the concentrator. The radiative cooler is on the back side of the PV module and has thermal radiation on both sides. The high solar spectrum transmission of the multi-layer low-iron soda lime glass cooler allows the concentrator right beneath the cooler to collect the AM1.5D sunlight (dashed yellow lines) with little loss. The cooler and the PV module are assumed to be away from the concentrator so that the view factor from the cooler to the concentrator is 0.1. Dominant heat transfer terms are labeled and their explanations can be found in the text. (B). Overall flowchart to explain how the optical-electrical-thermal coupled simulation framework can find the equilibrium temperature of PV module precisely and self-consistently.

RADIATIVE COOLER DESIGN AND RESULTS

3.1 Radiative cooler design

Soda lime glass has been proposed as a good radiative cooler material for different applications due to its high mid-IR emittance [13,23]. A subclass, known as low-iron soda lime glass, has the additional benefit of high solar transmission,

allowing daytime radiative cooling even with direct sunlight. However, its emittance spectrum dips near 10 μm. As shown by the green curve in Fig. 2 (B), this dip in emittance overlaps with the range of the main atmospheric window from 8 to 13 μm (shaded blue), making the heat transfer between the cooler and the cold universe suboptimal. To fully utilize the main atmospheric window, the emittance of the low-iron soda lime glass in this range should be enhanced. It has been proposed that 2D photonic crystal structures can substantially enhance the emittance within the atmospheric window close to unity [13]. In this work, similar enhancement has been achieved via a different approach. Since the dip in emittance is caused by high reflection near 10 μm, an anti-reflection (AR) coating applied on top of the low-iron soda lime glass may reduce the reflection. As shown in Fig. 2 (A), a 2.28 μm thick porous low-iron soda lime glass on top serves as a broadband AR coating. The dielectric constant ϵ of the porous glass is modeled by Bruggeman approximation [24] as:

$$v_g \frac{\epsilon_g - \epsilon}{\epsilon_g + 2\epsilon} + (1 - v_g) \frac{\epsilon_a - \epsilon}{\epsilon_a + 2\epsilon} = 0, \tag{15}$$

where v_g and ϵ_g are the volume fraction and the dielectric constant for a spectral range of $0.31 - 300$ μm [25] of low-iron soda lime glass, respectively; $\epsilon_a = 1$ is the dielectric constant of the air. In this work, the volume fraction of glass was optimized to be $v_g = 0.25$. Compared with photonic crystal structures, porous AR coating is more feasible for large scale production, using fabrication techniques such as chemical etching and the sol-gel method [26].

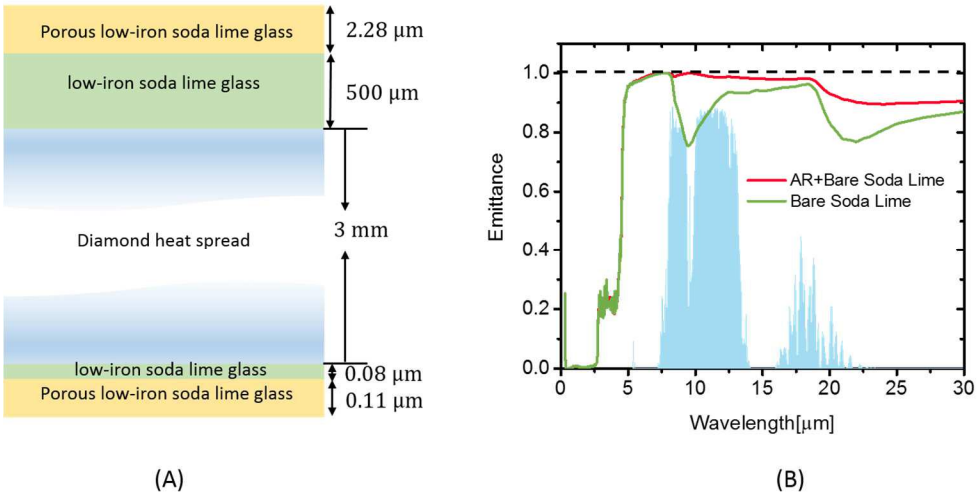

Figure 2. (A) Cross-sectional schematics of the multi-layer low-iron soda lime glass cooler. The 500 μm thick low-iron soda lime glass serves as the major cooling emitter. The 2.28 μm thick porous layer is a broadband anti-reflection (AR) coating that enhance the mid-IR emittance of the glass. The porous layer has an optimized glass volume faction of 25%. The 3 mm thick diamond layer is the transparent heat spreader that ensures both low non-uniformity in cooler temperature and high solar transmission. The two layers at the bottom is added to further increase the solar transmission of the cooler. The glass volume fraction of the bottom layer is the same as the top layer. (B) The simulated emittance spectrum of the multi-layer low-iron soda lime glass cooler (red) and the cooler without the porous layer (green). The porous low-iron soda lime glass layer can effectively enhance the emittance of the cooler within the $8 - 13$ μm atmospheric window (shaded blue).

Cooling with a high heat load often requires a larger cooler area than the heat source area (the PV module in HCPV). The geometry depicted in Fig. 1 could create non-uniform cooler temperatures over large areas. Thus, the one major assumption made in the calculation framework, $T_{cool} = T_{PV}$, may not be valid in all cases. Therefore, a 3D steady state thermal simulation using COMSOL Multiphysics was performed to evaluate the temperature gradient of the PV module + cooler structure. As shown in Fig. 3, the temperature gradient between the cooler and the PV module ($T_{PV} - T_{cool-ave}$) was calculated for different heat loads ($P_{in}^{PV} - P_{out}^{PV}$) and cooler areas ($A_{cool}$). T_{PV} was directly acquired from the simulation results, and $T_{cool-ave}$ was derived from the radiative power from the cooler surface by Stefan-Boltzmann law. Across the full range of heat loads and cooler areas considered in this work (i.e. below the dashed line in Fig. 3), a 3 mm thick diamond layer has a maximum temperature gradient less than 7 K, and usually much less.

Based on this result, a 3 mm thick diamond heat spreader was added at the bottom of the 500 μm-thick low-iron soda lime glass layer. The diamond layer performs two functions: (1) decreasing the radial temperature gradient of the cooler; and (2) maintaining the high solar transmission of the cooler, so that even the concentrator right below the cooler can collect sunlight. The dielectric constant of diamond in the spectral range of $0.31 - 20$ μm is from Reference [27,28] and was extrapolated as a constant between $20 - 300$ μm to match the spectral range of low iron soda lime glass. The extrapolation may lead to an error of a few percent in the net cooling power from the cooler. It is likely that a 3 mm thick diamond layer is unrealistic for mass production. However, it could be replaced by a thicker layer of other transparent thermal conductors, such as transparent conductive oxides, which can be deposited using roll-to-roll methods, such as knife-over-edge coating, slot-die coating and screen printing [29]. Other materials, such as an optical transmissive and thermally conductive network of metallic nanowires [30], may also be good candidates. To further enhance the solar transmission, two thin layers of low-iron soda lime glass and its porous layer with thicknesses labeled in Fig. 2 (A) were also added at the bottom.

The angular-dependent emittance spectra of the multi-layer low-iron soda lime glass cooler was simulated using S4 [31] across a broad range of wavelengths from 0.31 μm to 300 μm. The normal emittance spectrum of the multi-layer low-iron soda lime glass cooler is shown in Fig. 2 (B) in red. Compared with the bare low-iron soda lime cooler (green curve), the multi-layer low-iron soda lime glass cooler exhibits enhanced mid-IR emittance, especially in the atmospheric window. In tandem, the solar absorptance is designed to reach a low level, to allow radiative cooling in direct sunlight.

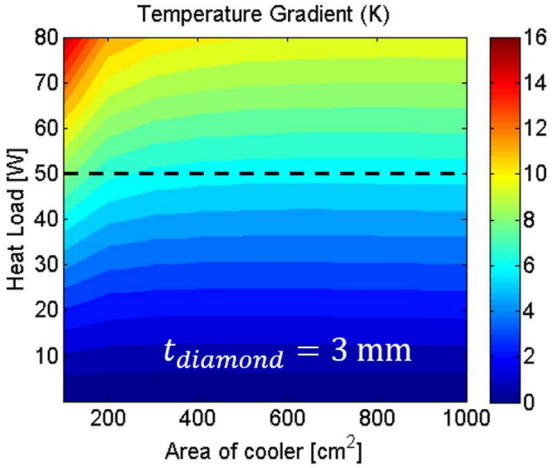

Figure 3. Steady state temperature gradient between the cooler and the PV module. The cooler temperature is the averaged value calculated from the radiated power by Stefan-Boltzmann law. For a 3 mm thick diamond heat spreader, the maximum temperature gradient is less than 7 K in the range of heat load and cooler area considered in this work (the contour below the black dashed line). Therefore, the approximation of $T_{PV} = T_{cool}$ is valid when a diamond heat spreader of 3 mm thick is used.

3.2 Results and Discussion

The performance of the proposed radiative cooler is examined by the calculation framework introduced in Section 2. Fig. 4 shows the PV module temperatures are evaluated for different combinations of radiative cooler area A_{cool} and actual concentration factors C_{actual}. Two cases are considered for comparison: (1) a multi-layer low-iron soda lime glass cooler and (2) a conventional copper cooler with its polished highly reflective top surface ($\rho = 0.95$) facing towards the sky, with its emissive oxidized back surface ($\varepsilon = 0.78$[14]) facing the ground. The front surface of the copper cooler should not be oxidized because its strong solar absorption will more than offset the radiative cooling effect at the target temperature of 60 ℃ (333.15 K) [14,32]. For any concentration factor used in the calculation, the radiative cooler is set to be smaller than the concentrator. Therefore, only the lower half of the contour in Fig. 4 is calculated. When multi-layer low-iron soda lime glass cooler is used, as shown in Fig. 4 (A), the PV module temperature T_{PV} goes up as the concentration factor increases, especially when the radiative cooler area is small. However, for larger radiative cooler areas, T_{PV} can reach well below the target temperature – as low as 308 K in the best case. As shown in Fig. 4 (B), the copper cooler has a higher temperature for the same cooler area and actual concentration factor. The lowest temperature

is 322 K, 14 K higher than the multi-layer low-iron soda lime glass cooler. Considering the highest temperature reached by either cooler (indicated by the arrow towards the bottom-right corner of each contour), the multi-layer low-iron soda lime glass cooler performs better as well; the maximum T_{PV} is 73 K lower. In both cases, the target temperature of 333.15 K is highlighted by a dashed line. The better cooling effect of the multi-layer low-iron soda lime glass cooler is also reflected in the more gradual slope of the dashed line, indicating more cooling power per unit area.

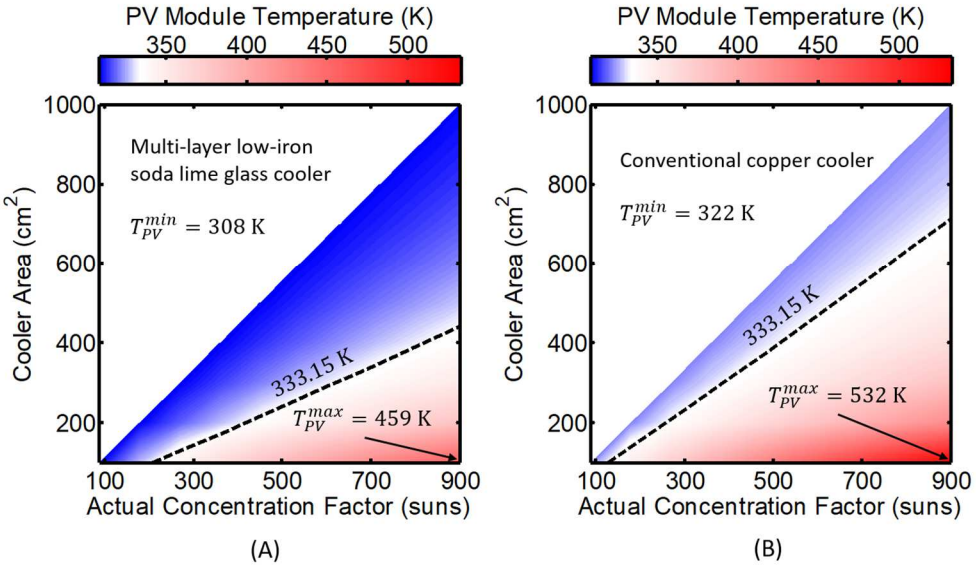

Figure 4. The simulated contour map of PV module temperature as a function of cooler area and actual concentration factor. The cooler area is always smaller than the concentrator area. (A) Multi-layer low-iron soda lime glass cooler. The minimum temperature it can reach is 308 K and the maximum 459 K. The dashed line shows the cooler area required for the target temperature of 333.15 K at different concentrations. (B) Conventional copper cooler. The minimum temperature it can reach is 322 K and the maximum 532 K. The dashed line shows the cooler area required for the target temperature of 333.15 K at different concentrations. It is obvious that the multi-layer low-iron soda lime glass cooler outperforms the copper cooler. For the same target temperature, less area of multi-layer low-iron soda lime glass cooler is required.

For concentrating photovoltaics (CPV) applications, especially HCPV, the weight of the cooler is a critical quantity, because a solar tracking system is generally needed [33]. Therefore, we proposed a figure of merit, the cooling power per weight [W/kg], by which different coolers can be compared quantitatively. The cooling power is the net output power from the cooler, $P_{out}^{cool} + P_{non-rad}^{PV,cool} - P_{in}^{cool}$, including radiation and convection. For the weight calculation, we assume that the copper cooler has the same thickness (3 mm) as the diamond heat spreader. The densities of the materials are listed in Table 1.

Table 1 Densities of the cooler materials

Material Density [kg/m^3]			
Multi-layer low-iron soda lime glass cooler		**Conventional copper cooler**	
Porous low-iron soda lime glass	633		
Low-iron soda lime glass	2530	Copper	8960
Diamond	3510		

For the two different coolers investigated, their weight and cooling power per weight are calculated at different actual concentration factors and PV module temperature of 333.15 K. From Fig. (5), it is obvious that the weight of the conventional copper cooler (orange dashed line with triangle symbol) increases faster than the multi-layer low-iron soda lime glass cooler (orange solid line with square symbol). The derived cooling power per weight of each cooler is shown by blue line in Fig. (5). The introduced figure of merit clearly has a weak dependence on concentration factors, allowing it to be used as a cooler index applicable for a broad range of concentration. From Fig. (5), the cooling power per weight of the multi-layer low-iron soda lime glass cooler (blue solid line with square symbol) is around 3.7 times higher than that of the copper cooler (blue dashed line with triangle symbol), greater than the density ratio of copper to the diamond, due to the capability of radiative cooling under direct sunlight. Therefore, for the same actual concentration factor and target temperature, less weight of the cooler will be added to the solar tracking system if the multi-layer low-iron soda lime glass cooler is used. Aluminum, as another popular material used for HCPV coolers, is in many cases more favorable due to its lower density ($2700\ \mathrm{kg/m^3}$) compared with copper. However, the thermal conductivity of aluminum ($205\ \mathrm{W/m \cdot K}$) is lower than copper as well. Therefore, a thicker aluminum cooler should be used for a flat heat sink to achieve similar temperature uniformity. Considering both factors, the cooling power per weight of aluminum cooler should be higher than the copper cooler, but not as high as the multi-layer low-iron soda lime glass cooler when evaluated using the framework introduced in Section 2. It should be noted as well that the area of the concentrator is not considered in the figure of merit yet. The fact that copper or aluminum, unlike the multi-layer low-iron soda lime glass cooler, is not transparent to sunlight results in a larger concentrator area to achieve the same amount of actual concentration. This may lead to an even heavier HCPV system to be mounted on the solar tracker. For this work, the focus is on the cooler design. So the quantitative comparison was restricted to the cooler only. But it will be an interesting assessment if the entire HCPV system can be considered in future works.

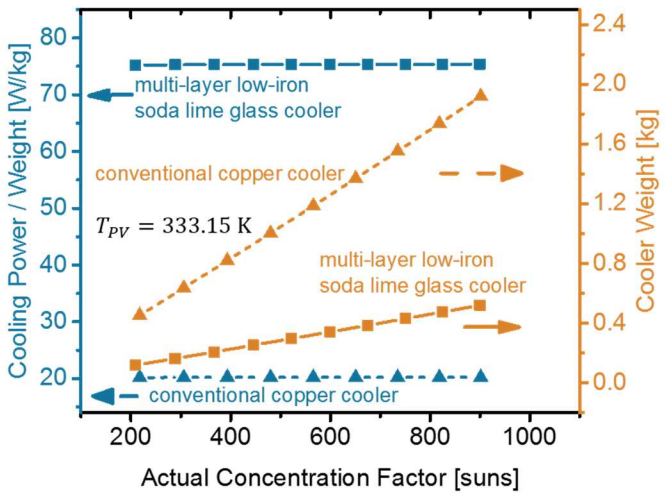

Figure 5. The figure of merit (blue lines) and cooler weight (orange lines) comparison between the multi-layer low-iron soda lime glass cooler and the conventional copper cooler. The cooling power is the net cooling power (radiation + convection) from the cooler. For copper cooler, the thickness is assumed to be 3 mm thick to match with the diamond heat spreader. The figure of merit is evaluated at the target temperature of 333.15 K [32]. The advantage of the multi-layer low-iron soda lime glass cooler (solid blue line with square symbol) is significant: the cooling power per weight is around 3.7 times higher than that of the copper cooler (dashed blue line with triangle symbol), greater than the density ratio between copper and diamond. Furthermore, much less concentrator area is needed when multi-layer low-iron soda lime glass cooler is used, because of its high solar transmission.

CONCLUSIONS

The application of radiative cooling within the atmospheric window in the infrared to high-concentration photovoltaic (HCPV) systems has been investigated. Using a realistic, self-consistent simulation framework, a multi-layer low-iron soda lime glass cooler has been designed. Its porous AR coating enhances the mid-IR emittance, allowing radiative cooling under direct sunlight. Furthermore, the proposed cooler is mostly transparent, with high solar transmission. Even a large cooler area blocks very little solar irradiance for concentration. It is shown that a PV module temperature as low as 308 K (about 15 K above ambient) can be reached when the multi-layer low-iron soda lime glass cooler is used, assuming the cooler is no larger than the concentrator. When compared with a conventional copper cooler, it is found that a much smaller area of multi-layer low-iron soda lime glass cooler is now needed to reach the standard HCPV module target temperature of 333.15 K. To account for the weight of the cooler that may affect the solar tracking system, a figure of merit, cooling power per weight, is introduced to evaluate each cooler quantitatively. For all the concentration factors considered (200 to 900 suns) while operating at the temperature of 333.15 K, the cooling power per weight of the multi-layer low-iron soda lime glass cooler is found to be around 3.7 times higher than that of the conventional copper cooler, and is also expected to be higher than an aluminum cooler. While the initial design uses diamond, there is also potential to shift to lower-cost transparent, thermally-conductive materials. Therefore, radiative cooling has a potential of being applied as a major or complementary cooling method for HCPV systems. Experimental verification would be warranted to help fully confirm the feasibility of low-cost, high performance radiative cooling enabled HCPV systems.

REFERENCES

[1] Trombe, F., "Perspectives sur l'utilisation des rayonnements solaires et terrestres dans certaines régions du monde," Rev. Gen. Therm. **6**(70), 1285 (1967).

[2] Bartoli, B., Catalanotti, S., Coluzzi, B., Cuomo, V., Silvestrini, V.., Troise, G., "Nocturnal and diurnal performances of selective radiators," Appl. Energy **3**(4), 267–286 (1977).

[3] Granqvist, C. G.., Hjortsberg, A., "Radiative cooling to low temperatures : General considerations and application to selectively emitting SiO films," J. Appl. Phys. **52**(6), 4205 (1981).

[4] Catalanotti, S., Cuomo, V., Piro, G., Ruggi, D., Silvestrini, V.., Troise, G., "The radiative cooling of selective surfaces," Sol. Energy **17**(2), 83–89 (1975).

[5] Granqvist, C. G., Hjortsberg, A.., Eriksson, T. S., "Radiative cooling to low temperatures with selectively IR-emitting surfaces," Thin Solid Films **90**, 187–190 (1982).

[6] Gentle, A. R.., Smith, G. B., "Radiative Heat Pumping from the Earth Using Surface Phonon Resonant Nanoparticles," Nano Lett. **10**, 373–379 (2010).

[7] Yeng, Y. X., Ghebrebrhan, M., Bermel, P., Chan, W. R., Joannopoulos, J. D., Soljacic, M.., Celanovic, I., "Enabling high-temperature nanophotonics for energy applications," Proc. Natl. Acad. Sci. **109**(7), 2280–2285 (2012).

[8] Ghebrebrhan, M., Bermel, P., Yeng, Y., Celanovic, I., Soljačić, M.., Joannopoulos, J., "Tailoring thermal emission via Q matching of photonic crystal resonances," Phys. Rev. A **83**, 33810 (2011).

[9] Raman, A. P., Anoma, M. A., Zhu, L., Rephaeli, E.., Fan, S., "Passive radiative cooling below ambient air temperature under direct sunlight," Nature **515**(7528), 540–544 (2014).

[10] Chen, Z., Zhu, L., Raman, A.., Fan, S., "Radiative cooling to deep sub-freezing temperatures through a 24-h day-night cycle," Nat. Commun. **7**, 13729 (2016).

[11] Zhai, Y., David, S. N., Zhao, D., Lou, R., Tan, G.., Yang, R., "Scalable-manufactured randomized glass-polymer hybrid metamaterial for daytime radiative cooling," Science (80-.). **355**, 1062–1066 (2017).

[12] Zhu, L., Raman, A. P.., Fan, S., "Radiative cooling of solar absorbers using a visibly transparent photonic crystal thermal blackbody.," Proc. Natl. Acad. Sci. U. S. A. **112**(40), 12282–12287 (2015).

[13] Zhou, Z., Sun, X.., Bermel, P., "Radiative cooling for thermophotovoltaic systems," Infrared Remote Sens. Instrum. XXIV **9973**, M. Strojnik, Ed., 997308 (2016).

[14] Micheli, L., Fernández, E. F., Almonacid, F., Mallick, T. K.., Smestad, G. P., "Performance , limits and economic perspectives for passive cooling of High Concentrator Photovoltaics," Sol. Energy Mater. Sol. Cells **153**, 164–178 (2016).

[15] Sun, X., Silverman, T. J., Zhou, Z., Khan, M. R., Bermel, P.., Alam, M. A., "Optics-Based Approach to Thermal Management of Photovoltaics: Selective-Spectral and Radiative Cooling," IEEE J. Photovoltaics **7**(2), 566–574 (2017).

[16] Araki, K., Uozumi, H.., Yamaguchi, M., "A simple passive cooling structure and its heat analysis for 500 x concentrator PV module," Proc. Twenty-Ninth IEEE Photovolt. Spec. Conf., 1568–1571 (2002).

[17] Gualdi, F., Arenas, O., Vossier, A., Dollet, A., Aimez, V.., Arès, R., "Determining Passive Cooling Limits In CPV Using An Analytical Thermal Model," AIP Conf. Proc., **1556**, 10–13 (2013).
[18] Natarajan, S. K., Mallick, T. K., Katz, M.., Weingaertner, S., "Numerical investigations of solar cell temperature for photovoltaic concentrator system with and without passive cooling arrangements," Int. J. Therm. Sci. **50**(12), 2514–2521 (2011).
[19] Green, M. A., Emery, K., Hishikawa, Y., Warta, W., Dunlop, E. D., Levi, D. H.., Ho-baillie, A. W. Y., "Solar cell efficiency tables (version 49)," Prog. Photovoltaics Res. Appl. **25**, 3–13 (2017).
[20] Taguchi, M., Yano, A., Tohoda, S., Matsuyama, K., Nakamura, Y., Nishiwaki, T., Fujita, K.., Maruyama, E., "24 . 7 % Record Efficiency HIT Solar Cell on Thin Silicon Wafer," IEEE J. Photovoltaics **4**(1), 96–99 (2014).
[21] Rees, W. G., [Physical Principles of Remote Sensing], 3, revised ed., Cambridge University Press (2012).
[22] Min, C., Nuofu, C., Xiaoli, Y., Yu, W., Yiming, B.., Xingwang, Z., "Thermal analysis and test for single concentrator solar cells," J. Semicond. **30**(4), 44011 (2009).
[23] Gentle, A. R.., Smith, G. B., "Is enhanced radiative cooling of solar cell modules worth pursuing ?," Sol. Energy Mater. Sol. Cells **150**, 39–42 (2016).
[24] Landauer, R., "Electrical conductivity in inhomogeneous media," AIP Conf. Proc. **40**(2), 1–45 (1978).
[25] Rubin, M., "Optical properties of soda lime silica glasses," Sol. Energy Mater. **12**, 275–288 (1985).
[26] Chen, D., "Anti-reflection (AR) coatings made by sol - gel processes : A review," Sol. Energy Mater. Sol. Cells **68**, 313–336 (2001).
[27] Phillip, H. R.., Taft, E. A., "Analysis of Reflectance Data for Diamond," Phys. Rev. **136**(5A), A1445 (1964).
[28] D. Palik, E., [Handbook of Optical Constants of Solids], Burlington : Elsevier Science (1997).
[29] Krebs, F. C., "Polymer solar cell modules prepared using roll-to-roll methods: Knife-over-edge coating, slot-die coating and screen printing," Sol. Energy Mater. Sol. Cells **93**(4), 465–475 (2009).
[30] Wu, H., Kong, D., Ruan, Z., Hsu, P.-C., Wang, S., Yu, Z., Carney, T. J., Hu, L., Fan, S., et al., "A transparent electrode based on a metal nanotrough network," Nat. Nanotechnol. **8**(6), 421–425 (2013).
[31] Liu, V.., Fan, S., "S 4 : A free electromagnetic solver for layered periodic structures," Comput. Phys. Commun. **183**(10), 2233–2244 (2012).
[32] Kurtz, S., "Opportunities and Challenges for Development of a Mature Concentrating Photovoltaic Power Industry Opportunities and Challenges for Development of a Mature Concentrating Photovoltaic Power Industry" (2009).
[33] Pérez-Higueras, P., Muñoz-Rodríguez, F. J., Adame-Sánchez, C., Hontoria-García, L., Rus-Casas, C., González-Rodríguez, A., Aguilar-Peña, J. D., Gallego-Álvarez, F. J., González-Luchena, I., et al., [High-Concentrator Photovoltaic Power Plants: Energy Balance and Case Studies], Springer (2015).